IEEE Photonics Journal
An IEEE Photonics Society Publication

Open Access

N × N Reconfigurable Nonblocking Polymer/Silica Hybrid Planar Optical Switch Matrix Based on Total-Internal-Reflection Effect

Volume 9, Number 4, August 2017

L. Liang
K. Zhang
C. T. Zheng
X. Zhang
L. Qin
Y. Q. Ning
D. M. Zhang
L. J. Wang

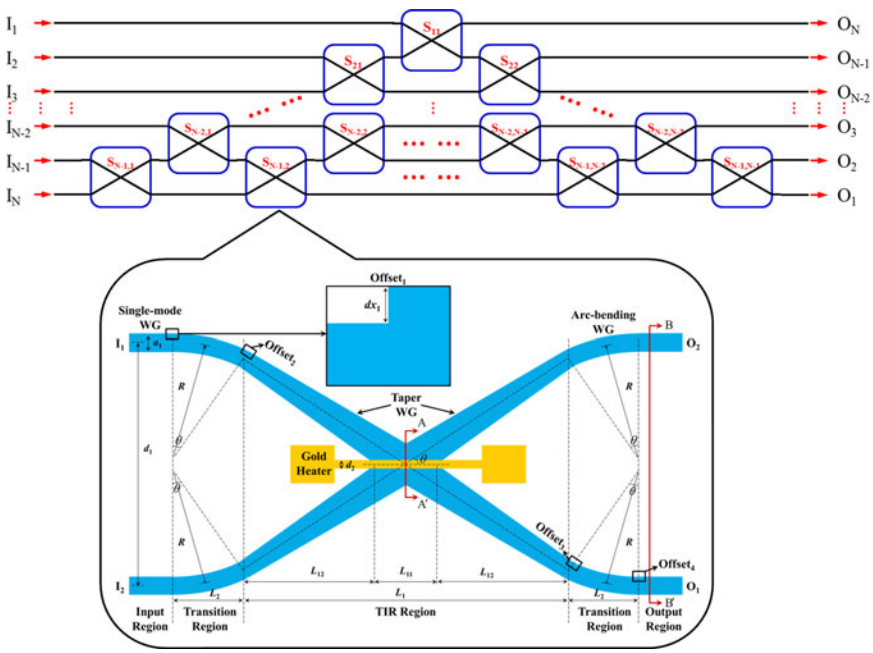

DOI: 10.1109/JPHOT.2017.2718019
1943-0655

N × N Reconfigurable Nonblocking Polymer/Silica Hybrid Planar Optical Switch Matrix Based on Total-Internal-Reflection Effect

L. Liang,[1] K. Zhang,[1] C. T. Zheng,[2] X. Zhang,[1] L. Qin,[1] Y. Q. Ning,[1] D. M. Zhang,[2] and L. J. Wang[1]

[1]State Key Laboratory of Luminescence and Applications, Changchun Institute of Optics Fine Mechanics and Physics, Chinese Academy of Sciences, Changchun 130033, China
[2]State Key Laboratory on Integrated Optoelectronics, College of Electronic Science and Engineering, Jilin University, Changchun 130012, China

DOI:10.1109/JPHOT.2017.2718019

Manuscript received April 7, 2017; revised June 14, 2017; accepted June 16, 2017. Date of publication June 21, 2017; date of current version June 30, 2017. This work was supported in part by the National Science Foundation Council of China (Nos. 61234004, 61604151, 51672264, 61474118, 61474117), in part by the Science and Technology Development Plan of Jilin University (Nos. 20160520017JH and 20150520104JH), in part by the National Key Research and Development Program of China (Nos. 2016YFE0126800), and in part by the open project of the State Key Laboratory of Luminescence and Applications. Corresponding authors: X. Zhang and D. M. Zhang (e-mail: zhangx@ciomp.ac.cn; zhangdm@jlu.edu.cn.)

Abstract: We present a reconfigurable model for N × N non-blocking optical switch matrix (OSM) constituted by N(N-1)/2 2 × 2 thermo-optic polymer/silica hybrid total-internal-reflection switch elements. The number of the elements in the general model is reduced by about 50% compared to the reported all nonblocking OSM, in addition, the proposed model is more compact in footprint and more power-efficient. Each element consists of crossed multimode polymer/silica hybrid waveguides and a heater electrode at the switching node. A switching power of 53.9 mW is required at 1550-nm wavelength to drop the crosstalk below −28.0 dB. Measurements result in a rise time of 421.5/410.1 μs (O_1/O_2), a fall time of 534.2/464.6 μs (O_1/O_2), and crosstalk of −27.6 and −29.1 dB under cross state and bar state, respectively. Subtracting coupling losses, propagation losses of the device under cross state and bar state are about 1.0 and 1.8 dB, respectively. The fabricated 3 × 3 and 4 × 4 reconfigurable non-blocking OSMs using three and six switch elements at sizes of 16.0 mm × 6.8 mm and 26.0 mm × 6.8 mm all show excellent switching performances, and the insertion losses are less than 3.6 and 7.2 dB, respectively.

Index Terms: Non-blocking, optical switch matrix (OSM), total-internal-reflection (TIR), waveguide.

1. Introduction

Photonic networks-on-chip (NoCs) is an attractive option for chip-level communication in high performance chip multiprocessors (CMPs) for increasing the bandwidth, lowering the latency and reducing the power [1]. Power efficient and compact-sized optical switch matrix (OSM) is a key signals-switching device in the complex optical networks. Several optical structures for constructing an OSM, such as Mach-Zehnder interferometers (MZIs) [2], multimode interferometers (MMIs)

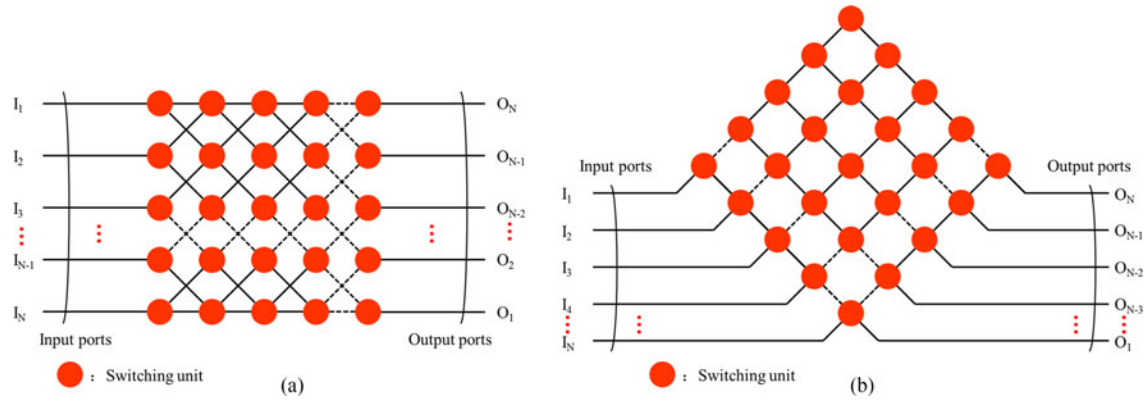

Fig. 1. Two typical non-blocking architectures of optical switch matrixes, (a) mesh-type, (b) reflection-type.

[3]–[5], directional couplers (DCs) [6], and microring resonators (MRRs), have been demonstrated by using integrated planar lightwave circuit (iPLC) technology. However, those devices with too sophisticated structures are inherently sensitive to wavelength and fabrication tolerance. To overcome these limitations, a total-internal-reflection (TIR) OSM can be a promising candidate [7], [8]. On the other hand, by virtue of large thermo-optic (TO) coefficient of polymer and large thermal conductivity of silica, a polymer/silica hybrid waveguide structure, which was designed as MZI and MMI TO switches in our previous reports [9], can be more adaptive to TIR switches and related OSMs [8]. Moreover, polymer/silica hybrid TIR switches can be integrated with silicon based complementary metal–oxide–semiconductor (CMOS) integrated circuits and have the potential for cost effective mass production.

For an N × N non-blocking OSM in photonic NoCs, optical interconnect topologies must obey the following rules: 1) Light injected into the input of any one port can be guided to the output of any ports. 2) Any optical link between the input of one port and any output port would never block any possible optical links between the remaining input ports and output ports [10]. However, the implementing of N × N non-blocking OSM on planar waveguides is difficult for large port counts due to insertion losses of the switch elements. Until now, several non-blocking OSM architectures have been demonstrated by N^2 optical switches [11]–[14]. Fig. 1(a) and (b) are two typical architectures in which every node is a switch element. Here the number of switch elements within an optical path inducing large insertion loss as well as loss variations will increases power consumption and additional costs for too many useless switch units.

In this work, a reconfigurable model for N × N non-blocking OSM constituted by $N(N-1)/2$ 2 × 2 TO polymer/silica hybrid TIR switch elements is proposed. The switch element has low power consumption and fast response speed due to high TO coefficient of polymer and large thermal conductivity of silica. Using this reconfigurable model, 3 × 3 and 4 × 4 OSMs are demonstrated, their excellent non-blocking switching performances are showed by exhausting all optical links in each switching state.

2. Design of 2 × 2 TIR TO Switch

2.1 Device Structure

Fig. 2(a) shows the schematic diagram of the 2 × 2 polymer/silica hybrid TIR TO switch, which consists of six components, including single mode input/output waveguides, two transition regions, TIR region, and Au heater. Four arc-bending waveguides are used in the two transition regions. Au electrode heater for realizing good mode transmission and reflection operations by TO effect is on an X-junction that is made up of four taper waveguides in the TIR region. The material parameters about refractive index (RI), thermal conductivity (TC), TO coefficient dn/dt, density ρ, and heat

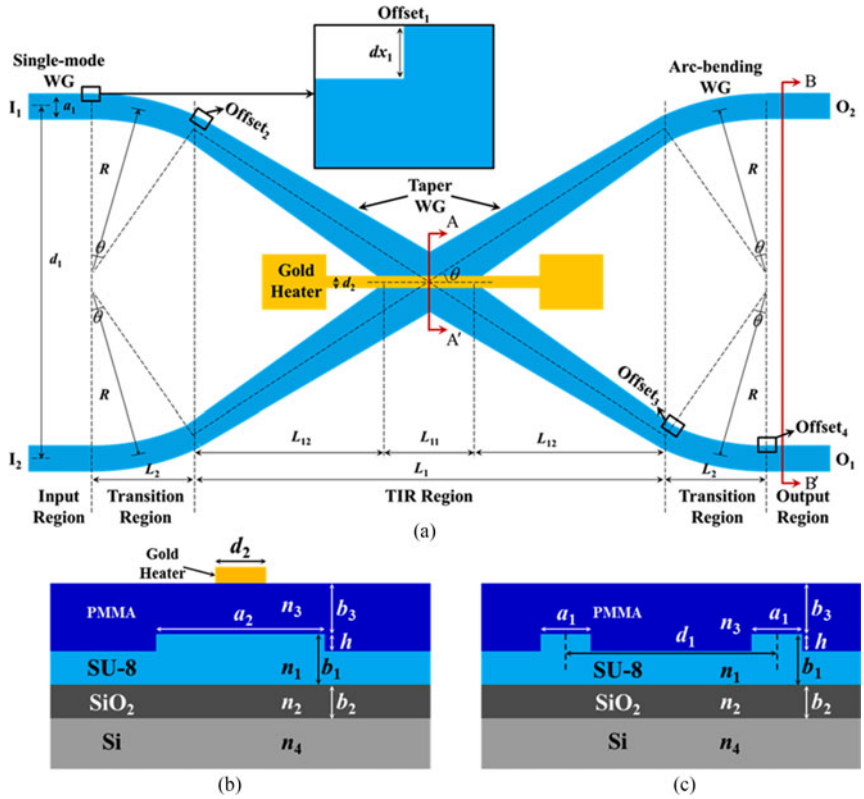

Fig. 2. (a) Schematic diagram, (b) cross-section view A-A' over the cross-point in the TIR region, and (c) cross-section view B-B' in the output region of the 2 × 2 polymer/silica hybrid TIR TO switch.

TABLE 1
Parameters of Adopted Materials in Our TIR Switch Element at 1550 nm and 300 K

Material	RI	TC ($WK^{-1}m^{-1}$)	dn/dt (K^{-1})	P ($kg.m^{-3}$)	c_p ($J.kg^{-1}.K^{-1}$)
SU-8	1.573	0.2	$-1.8 \times 10-4$	1190	1200
P(MMA-GMA)	1.483	0.19	$-1.2 \times 10-4$	1190	1420
Silica	1.444	1.4	$1.0 \times 10-5$	2200	730
Silicon	3.45	131	$1.86 \times 10-4$	2329	700
Gold	0.19	317	—	19300	129

capacity c_p of SU-8 2002, P(MMA-GMA), silica, silicon, and gold at 1550 nm and 300 K are listed in Table 1.

The waveguide cross sectional view $A - A'$ in the X-junction region and $B - B'$ in the output region are shown in Fig. 2(b) and (c). The proposed device works at 1550 nm wavelength, it should be ensured that the input and output waveguides satisfy the single-mode condition. Fig. 3(a) exhibits the simulated relationship between effective refractive index Neff and rib waveguide width a1 at different modes when $h = a_1/3$ and $b = a_1$. As can be seen, when a1 is less than 3 μm, the waveguide only has E_{00}^{y} fundamental mode. The optical mode field distribution of the waveguide profile simulated by RF module of COMSOL Multiphysics is shown in Fig. 4(a).

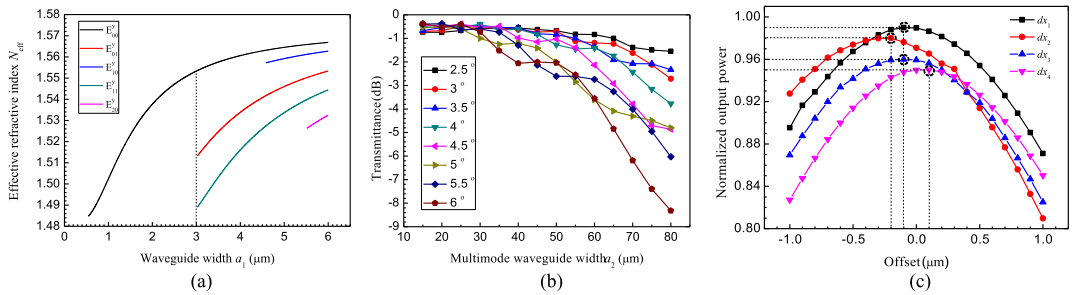

Fig. 3. Structure optimization of the TIR switch element, (a) effective refractive index N_{eff} as a function of core waveguide width a_1 of the five high-order modes for the input/output waveguides. (b) Transmittance of light passing through the crossed multimode waveguide whose width is a_2. (c) Normalized output power passing through four junctions $dx_1 \sim dx_4$ in the waveguide I_1-O_1.

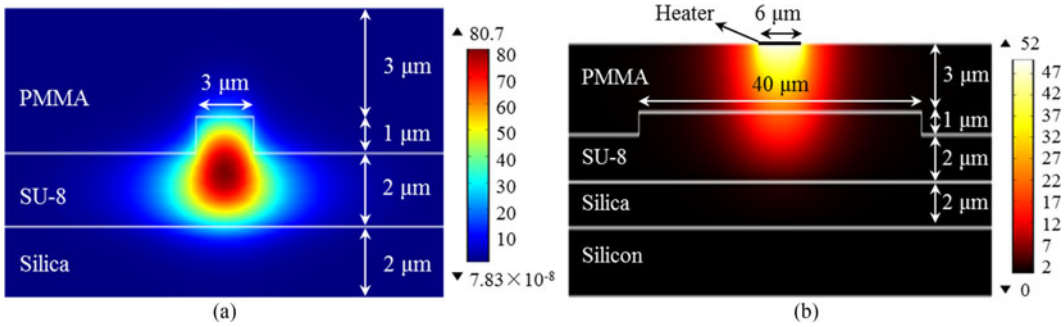

Fig. 4. The mode field distribution of the 3 μm-wide waveguide and (b) heat distribution over the waveguide cross-section.

The distance between two input/output waveguides is designed as $d_1 = 250\,\mu$m to match general standard optical fiber array. The radius of each arc-bending waveguide is $R = 10$ mm. The central Angle of each arc-bending segment is equal to the half crossing angle θ of the X-junction. By varying the width of the X-junction, an optimal transmittance is obtained when $\theta = 3.5^\circ$ and $a_2 = 40\,\mu$m as can be seen in Fig. 3(b). Here the three horizontal lengths L_{11}, L_{12} and L_2 related to the device size are decided by θ.

A mode matching method will be used to find optimal values for the segment offsets. At each junction among the segments in the waveguide I_1-O_1, the overlap integral of the input segment mode and the output segment mode will be maximized by varying the offset between the two segments. The mode of each segment will be calculated, and then a beam propagation method (BPM) simulation will be set up such that it returns the value of the overlap by scanning over the first variable $Offset_1$, which is the value of the offset between the straight input waveguide and the first arc waveguide. Here, in the same manner, other processes need to be repeated thrice more for the remaining junctions defined as $Offset_2$, $Offset_3$, and $Offset_4$ in the rest I_1-O_1. From the results in Fig. 3(c), it is easy to see that the best coupling position occurs at the peak of each curve, and the optimal values of the offsets are found to be $Offset_1 = -0.1\,\mu$m, $Offset_2 = -0.2\,\mu$m, $Offset_3 = -0.1\,\mu$m, $Offset_4 = 0.1\,\mu$m, respectively. Similarly, the optimal values of the offsets in the other waveguide I_2-O_2 are 0.1 μm, 0.2 μm, 0.1 μm and -0.1 μm according to the symmetry of the 2 × 2 TIR TO switch, respectively. As a result, the maximum transmission loss caused by the junctions of each switch element will be lowest.

2.2 Simulation on Switching Function

The template is used to format your paper and style the text. All margins, column widths, line spaces, and text fonts are prescribed; please do not alter them. You may note peculiarities. For

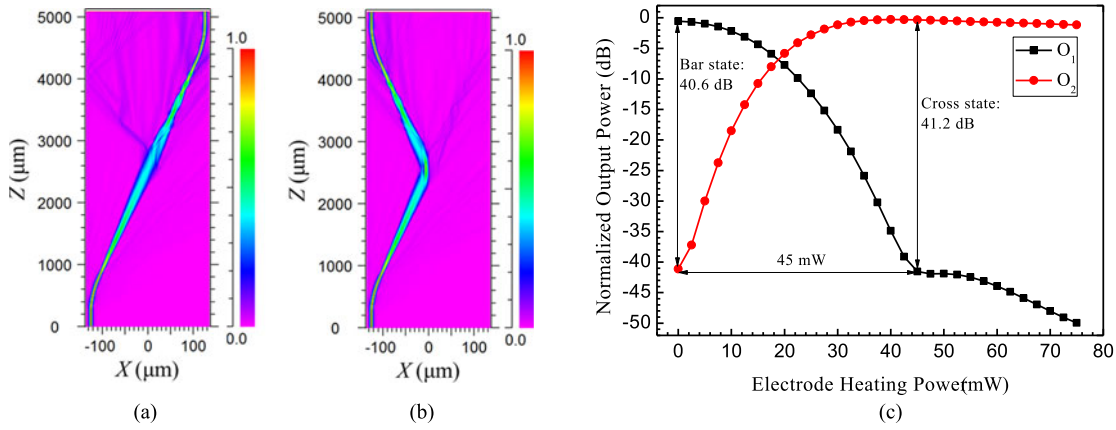

Fig. 5. Propagation powers of the TIR switch under (a) cross state and (b) bar state. (c) Simulated curves of output power versus driving power.

example, the head margin in this template measures proportionately more than is customary. This measurement and others are deliberate, using specifications that anticipate your paper as one part of the entire proceedings, and not as an independent document. Please do not revise any of the current designations.

The temperature distribution of the multimode waveguide in transversal surface can be obtained by solving the following heat transfer equation

$$\rho c_p \frac{\partial T}{\partial t} = \dot{q} + \frac{\partial}{\partial x}\left(k_x \frac{\partial T}{\partial x}\right) + \frac{\partial}{\partial y}\left(k_y \frac{\partial T}{\partial y}\right) + \frac{\partial}{\partial z}\left(k_z \frac{\partial T}{\partial z}\right) \tag{1}$$

where $\dot{q}$ is the heat generation rate per unit volume (its unit is W·cm-3), and k_x, k_y and k_z are thermal conductivities in x, y and z direction, respectively. Fig. 4(b) shows the calculated steady-state thermal field distribution when the heating temperature on electrode is 50 K. It is a hypothesis that the temperature change of every point of the waveguide in transversal surface is $\Delta T(x, y)$, and the refractive index variation at the point is

$$\Delta n\,(x, y) = n_T\,(x, y) \times \Delta T\,(x, y) \tag{2}$$

where $n_T(x, y)$ is the TO coefficient of the material at the corresponding coordinate. The refractive index variation in transversal surface can be obtained from the temperature change of the heating electrode, and then we can calculate the mode effective refractive index.

The simulated propagation powers along the waveguides are shown in Fig. 5(a) and (b). When no voltage is applied on the heating electrode of the switch element, defined as bar state, an incident light will be guided from an input port I_1/I_2 to an output port O_1/O_2. While applying a suitable thermal power in the heating electrode, defined as cross state, the incident light will be guided from the input port I_1/I_2 to the reflected output port O_2/O_1. The electrode heating power of the switch needed to realize the exchange between cross state and bar state defined as driving power. Fig. 5(c) shows the simulated curves of output power versus driving power, we can see that only a power of 45 mW is required to drop the crosstalk below −40 dB.

3. Device Fabrication and Measurement of 2 × 2 TIR TO Switch Element

3.1 Device Fabrication

A 2.0 μm thick silica under cladding layer was grown on silicon substrate by plasma enhanced chemical vapor deposition (PECVD). Then a 3.0 μm thick SU-8 layer was spun-coated on the under cladding. After soft bake, a 3.0 μm width rib waveguide with a rib height of 1.0 μm was

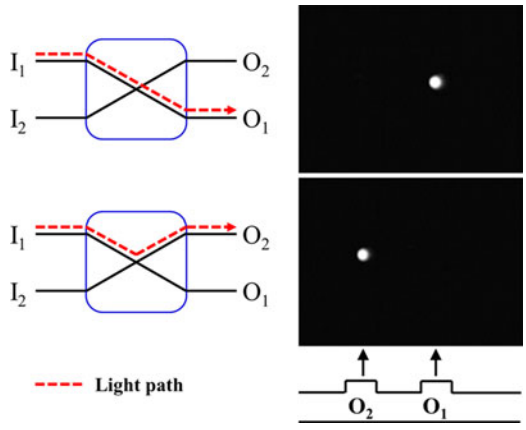

Fig. 6. Two light paths and the corresponding patterns under the two switching states.

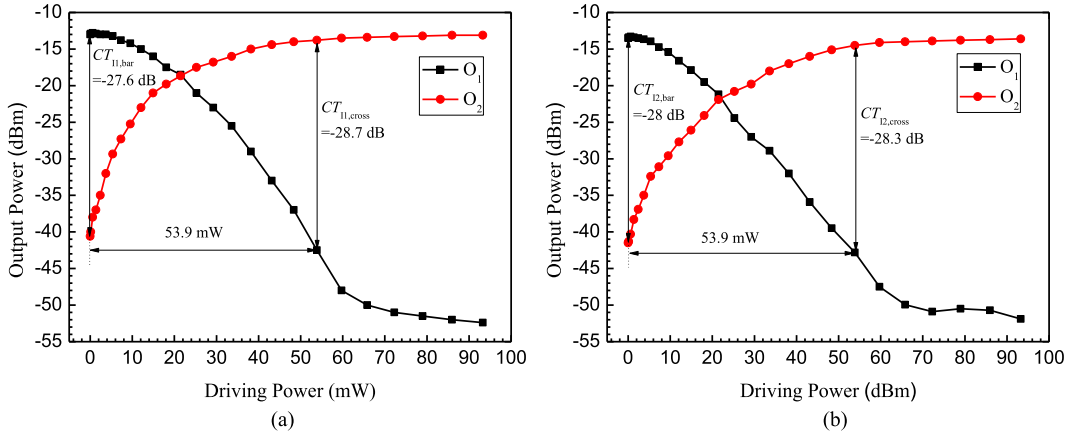

Fig. 7. Measured curves of output power versus driving power when the light is launched into the switch from input port I_1 (a) and I_2 (b).

formed by photolithography and wet etching process. Then the core film was hard-baked in order to sufficiently cross-link and obtain stable chemical and thermal features. Finally, a 3.0 μm thick PMMA film was spin-coated to form the upper cladding.

Upon the upper cladding, a 100 nm thick gold film was deposited through thermal evaporation approximately. Then, a lithography development process of a positive photoresist BP218 was completed under UV radiation using an electrode mask, and the sample was developed in NaOH solution with a concentration of 5‰. Gold electrode graphics were finally formed in iodine and potassium iodide solution (I: KI: H_2O = 1g: 4g: 50 ml). Fig. 6 shows the two light paths and the corresponding measured patterns under bar state and cross state.

3.2 Static and Dynamic Measurements

0 dBm of input power was coupled into input port I1 at wavelength of 1550 nm. The driving power is tuned by changing the supply voltage. As shown in Fig. 7(a), when the driving power equals 0 mW (bar state), O_1 and O_2 are −13.0 and −40.6 dBm, respectively. The total propagation loss and crosstalk are about 13.0 and −27.6 dB, respectively. As the driving power increases to 53.9 mW (cross state), O_1 and O_2 are −42.5 dBm and −13.8 dBm, respectively. The total propagation loss and crosstalk are about 13.8 and −28.7 dB, respectively. Subtracting fiber-to-chip and chip-to-fiber coupling losses measured by truncation method from the total propagation loss, we obtain 1.0 and 1.8 dB propagation losses under bar state and cross state for the 0.5 cm-long core switch element,

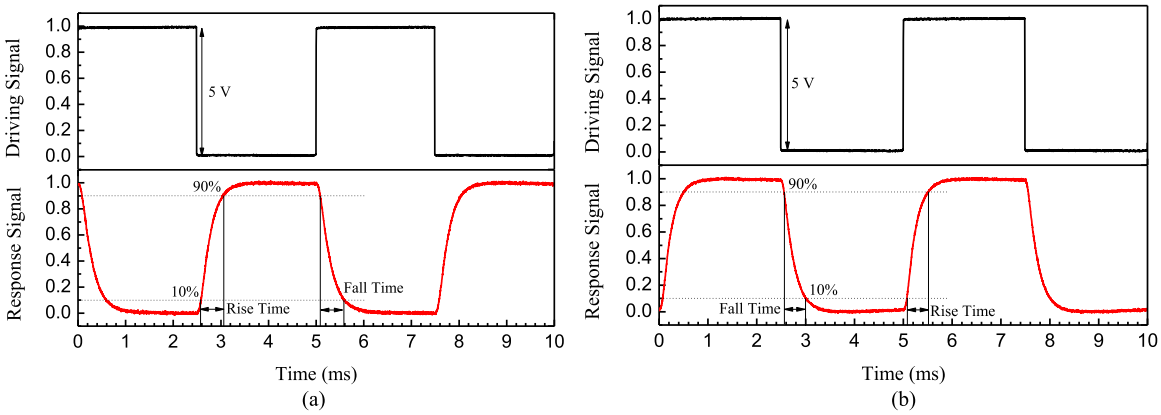

Fig. 8. Measured switching responses of the output powers (a) O_1 and (b) O_2. The upper black trace is the driving voltage signal. The lower red trace is the response signal.

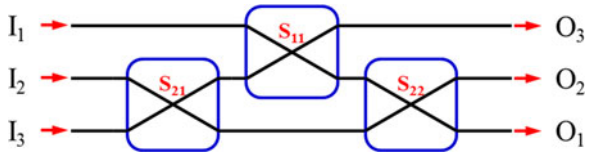

Fig. 9. 3 × 3 non-blocking optical switch array.

respectively. when the input light was coupled into port I_2, as shown in Fig. 7(b), the crosstalk are -28.0 and -28.3 dB under bar and cross state, respectively. The total propagation losses under bar and cross state are about 1.5 and 2.5 dB, respectively.

To measure the dynamic response, the output light was coupled into a photodiode detector connected to an oscilloscope. Under 200 Hz switching operation of a square-wave signal, the dynamic variation curves of O_1 and O_2 are shown in Fig. 8(a) and (b), respectively. The measured rise time and fall time of the TIR switch are about 421.5/410.1 and 534.2/464.6 μs, respectively. Compared with the phase-change-based MZI TO switch [9], the heat accumulation in the waveguide of the device is significantly larger, the response time is slower than the device fabricated with the same silica/polymer hybrid materials.

4. 3 × 3, 4 × 4, and N × N Reconfigurable Non-Blocking OSM Toplogy

4.1 3 × 3 Non-Blocking Optical Switch Array

A 3 × 3 optical switch array is proposed by using the rearranged N × N matrix schematic diagram as shown in Fig. 9. The device has a compact size of 16.0 mm × 6.8 mm consisting of three switch elements S_{11}, S_{21}, and S_{22}. There are 6 (3! = 6) states when the input port I_i (i = 1, 2, 3) and the output port Oj (j = 1, 2, 3) linked with each other as shown in the Table 2. When S_{11}, S_{21}, and S_{22} are all under bar state (b, b, b), we can see an optical link "$I_1 \rightarrow O_1$, $I_2 \rightarrow O_2$, $I_3 \rightarrow O_3$". The other optical links have similar operations. There are 2^3 operations of the combined elements, and the fifth and sixth state both have two switch operations. Considered with power consumption, when S_{11}, S_{21}, and S_{22} are all under cross state (c, c, c) in state 6, all elements have power consumption. While on the other operation (c, b, b), it will be used preferentially because only one element has power consumption. It also can be seen that state 5 have two operations with same power consumption.

For achieving -25 dB crosstalk, a power consumption of 48 mW (cross state) is required for one switch element. Based on Table 2, within all optical links, the minimum and maximum numbers of the switch elements under cross state are 0 and 2, respectively, thus an average power consumption

TABLE 2
Non-Blocking Optical Links of 3 × 3 Optical Switch Array

State	Optical links	S_{11}	S_{21}	S_{22}
1	$I_1 \rightarrow O_1$, $I_2 \rightarrow O_2$, $I_3 \rightarrow O_3$	b	b	b
2	$I_1 \rightarrow O_2$, $I_2 \rightarrow O_3$, $I_3 \rightarrow O_2$	b	c	b
3	$I_1 \rightarrow O_2$, $I_2 \rightarrow O_1$, $I_3 \rightarrow O_3$	b	b	c
4	$I_1 \rightarrow O_2$, $I_2 \rightarrow O_3$, $I_3 \rightarrow O_1$	b	c	c
5	$I_1 \rightarrow O_3$, $I_2 \rightarrow O_1$, $I_3 \rightarrow O_2$	c	b/c	c/b
6	$I_1 \rightarrow O_3$, $I_2 \rightarrow O_2$, $I_3 \rightarrow O_1$	c	b(c)	b(c)

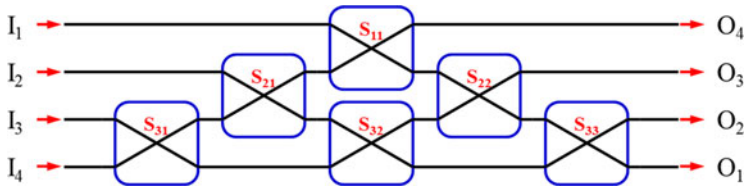

Fig. 10. 4 × 4 non-blocking optical switch array.

of 56 mW is needed. Under most optical links, the insertion losses are 2.0 ∼ 3.6 dB. Considering switching performance, this result is better than most of previous 3 × 3 optical switch arrays [5], [15], due to the adopted optimal TIR waveguide structure.

4.2 4 × 4 Non-Blocking Optical Switch Array

A 4 × 4 optical switch array including six 2 × 2 TIR TO switch elements defined as S_{11}, S_{21}, S_{22}, S_{31}, S_{32}, and S_{33} is also proposed in Fig. 10. There are 2^6 operations of the combined elements on the size of 26.0 mm × 6.8 mm. Considering that some operations construct one optical link state, only 24 (4! = 24) states were obtained. Subtracting the operations with more power consumption in parentheses as shown in Table 3, the minimum and maximum numbers of the switch elements under cross state are 0 and 4, respectively, thus an average power consumption of 104 mW is needed. Under most optical links, the insertion losses are 3.0∼7.2 dB. Compared with other works [7], [14], this 4 × 4 non-blocking optical switch array still has excellent competitiveness in switching performances.

4.3 N × N Non-Blocking OSM Topology

A conceptual schematic configuration of our N × N reconfigurable non-blocking OSM is illustrated in Fig. 11. As can be seen, a power-efficient non-blocking OSM should use as many passive optical links as possible. The improved architecture, obeying the rules of non-blocking OSM in Section 1, rearranges the OSM to have less number elements for all optical paths and greatly improves the loss uniformity. For input and output port number N, the OSM at least has N! states and needs $1 + 2 + \ldots\ldots + (N-2) + (N-1) = N(N-1)/2$ optical switch elements, which tends to have better power performance. As can be seen in Fig. 12, the number of the optical switches is reduced about 50% compared to the reported OSMs [13], [14]. 2 × 2 TO polymer/silica hybrid TIR switches are used as switch elements of the proposed OSM.

TABLE 3
Non-Blocking Optical Links of 4 × 4 Optical Switch Array

State	Optical links	S_{11}	S_{21}	S_{22}	S_{31}	S_{32}	S_{33}
1	$I_1 \rightarrow O_1$, $I_2 \rightarrow O_2$, $I_3 \rightarrow O_3$, $I_4 \rightarrow O_4$	b	b	b	b	b	b
2	$I_1 \rightarrow O_1$, $I_2 \rightarrow O_2$, $I_3 \rightarrow O_4$, $I_4 \rightarrow O_3$	b	b	b	c	b	b
3	$I_1 \rightarrow O_1$, $I_2 \rightarrow O_3$, $I_3 \rightarrow O_2$, $I_4 \rightarrow O_4$	b	b	b	b	c	b
4	$I_1 \rightarrow O_1$, $I_2 \rightarrow O_3$, $I_3 \rightarrow O_4$, $I_4 \rightarrow O_2$	b	b	b	c	c	b
5	$I_1 \rightarrow O_1$, $I_2 \rightarrow O_4$, $I_3 \rightarrow O_2$, $I_4 \rightarrow O_3$	b	c	b	b/c	c/b	b
6	$I_1 \rightarrow O_1$, $I_2 \rightarrow O_4$, $I_3 \rightarrow O_3$, $I_4 \rightarrow O_2$	b	c	b	b(c)	b(c)	b
7	$I_1 \rightarrow O_2$, $I_2 \rightarrow O_1$, $I_3 \rightarrow O_3$, $I_4 \rightarrow O_4$	b	b	b	b	b	c
8	$I_1 \rightarrow O_2$, $I_2 \rightarrow O_1$, $I_3 \rightarrow O_4$, $I_4 \rightarrow O_3$	b	b	b	c	b	c
9	$I_1 \rightarrow O_2$, $I_2 \rightarrow O_2$, $I_3 \rightarrow O_1$, $I_4 \rightarrow O_4$	b	b	b	b	c	c
10	$I_1 \rightarrow O_2$, $I_2 \rightarrow O_2$, $I_3 \rightarrow O_4$, $I_4 \rightarrow O_1$	b	b	b	c	c	c
11	$I_1 \rightarrow O_2$, $I_2 \rightarrow O_4$, $I_3 \rightarrow O_1$, $I_4 \rightarrow O_3$	b	c	b	b/c	c/b	c
12	$I_1 \rightarrow O_2$, $I_2 \rightarrow O_4$, $I_3 \rightarrow O_3$, $I_4 \rightarrow O_1$	b	c	b	b(c)	b(c)	c
13	$I_1 \rightarrow O_3$, $I_2 \rightarrow O_1$, $I_3 \rightarrow O_2$, $I_4 \rightarrow O_4$	b	b	c	b	b/c	c/b
14	$I_1 \rightarrow O_3$, $I_2 \rightarrow O_1$, $I_3 \rightarrow O_4$, $I_4 \rightarrow O_2$	b	b	c	c	b/c	c/b
15	$I_1 \rightarrow O_3$, $I_2 \rightarrow O_2$, $I_3 \rightarrow O_1$, $I_4 \rightarrow O_4$	b	b	c	b	b(c)	b(c)
16	$I_1 \rightarrow O_3$, $I_2 \rightarrow O_2$, $I_3 \rightarrow O_4$, $I_4 \rightarrow O_1$	b	b	c	c	b(c)	b(c)
17	$I_1 \rightarrow O_3$, $I_2 \rightarrow O_4$, $I_3 \rightarrow O_1$, $I_4 \rightarrow O_2$	b	c	c	b(b/c/c)	b(c/b/c)	b(c/c/b)
18	$I_1 \rightarrow O_3$, $I_2 \rightarrow O_4$, $I_3 \rightarrow O_2$, $I_4 \rightarrow O_1$	b	c	c	c/b/b(c)	b/b/c(c)	b/c/b(c)
19	$I_1 \rightarrow O_4$, $I_2 \rightarrow O_1$, $I_3 \rightarrow O_2$, $I_4 \rightarrow O_3$	c	b/b/b/c/c	b/c/c/b/b	c/b/b/b/c	b/b/c/c/b	c/c/b/b/b
20	$I_1 \rightarrow O_4$, $I_2 \rightarrow O_1$, $I_3 \rightarrow O_3$, $I_4 \rightarrow O_2$	c	b/c(b/b/c)	b/b(c/c/b)	b/b(c/c/c)	b/b(b/c/c)	c/b(c/b/b)
21	$I_1 \rightarrow O_4$, $I_2 \rightarrow O_2$, $I_3 \rightarrow O_1$, $I_4 \rightarrow O_3$	c	b/b(b/c/c)	b/c(c/b/b)	c/b(b/b/c)	b/b(c/c/b)	b/b(c/c/c)
22	$I_1 \rightarrow O_4$, $I_2 \rightarrow O_2$, $I_3 \rightarrow O_3$, $I_4 \rightarrow O_1$	c	b(b/b/c/c)	b(c/c/b/b)	b(c/c/b/c)	b(b/c/b/c)	b(b/c/c/c)
23	$I_1 \rightarrow O_4$, $I_2 \rightarrow O_3$, $I_3 \rightarrow O_1$, $I_4 \rightarrow O_2$	c	b/b/c(c/c/c)	b/b/c(c/c/c)	b/c/b(b/c/c)	c/c/b(c/b/c)	c/b/b(c/c/b)
24	$I_1 \rightarrow O_4$, $I_2 \rightarrow O_3$, $I_3 \rightarrow O_2$, $I_4 \rightarrow O_1$	C	b(b/c/c/c/c)	b(b/c/c/c/c)	b(c/b/b/c/c)	c(c/b/c/b/c)	b(c/c/b/b/c)

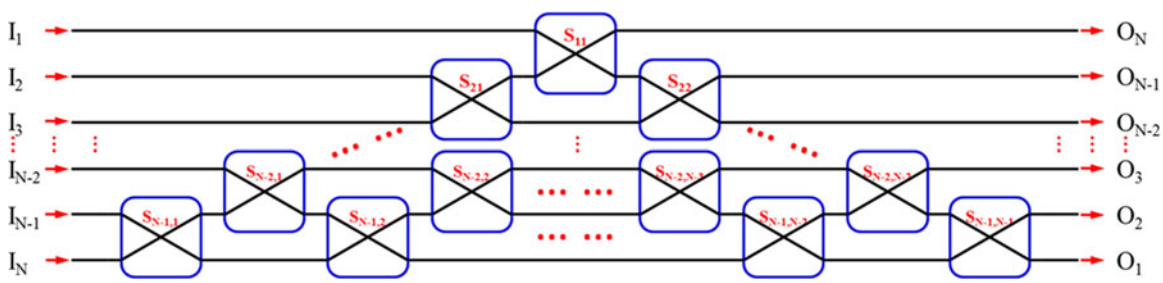

Fig. 11. Conceptual schematic configuration of N × N reconfigurable non-blocking OSM.

From the results of the 3 × 3, 4 × 4, and N × N OSMs, those using 2 × 2 TIR TO switch elements show excellent properties in terms of insertion losses, switching isolation, and power consumption. Furthermore, since they have a structural simplicity and compactness, our polymer/silica hybrid TIR TO switch arrays are believed to be well applicable for high-performance and low-cost optical switching networks.

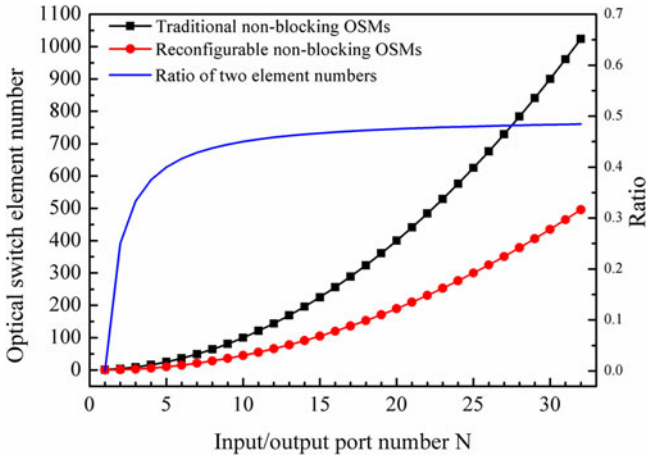

Fig. 12. A comparison of optical switch element number between traditional and reconfigurable non-blocking OSMs.

5. Conclusion

In summary, we demonstrated a reconfigurable N × N non-blocking OSM topology realized by using a 2 × 2 polymer/silica hybrid TIR TO switch as the unit switching element. The elements are distinctively composed of a plurality of crossed taper waveguides, gold heater electrodes in the switching node, and single mode waveguides in only the input/output regions. Through an optimization of the waveguide dimensions, cross angle, heater angle, and heater offset, we could obtain excellent optical properties in terms of the insertion loss, switching isolation, and power consumption. A switching power of 53.9 mW is required to drop the crosstalk below −28 dB. The 10–90% rise time and 90–10% fall time are 421.5/410.1 and 534.2/464.6 μs, respectively. By using 3 and 6 switch elements, compact non-blocking 3 × 3 and 4 × 4 OSMs with 2.0–3.6 dB and 3.0–7.2 dB propagation loss ranges for most optical links were proposed, and their average power consumptions are 56 and 104 mW, respectively. From this work, it is expected that the N × N OSM based on 2 × 2 polymer/silica hybrid TIR TO switches is scalable by our cascading approach and it is a promising way to realize low-power, low-loss, large-scale and cost-effective OSM to construct future highly-efficient photonic networks.

Acknowledgment

The authors wish to thank the anonymous reviewers for their valuable suggestions.

References

[1] A. Biberman, B. G. Lee, N. Sherwood-Droz, M. Lipson, and K. Bergman, "Broadband operation of nanophotonic router for silicon photonic networks-on-chip," *IEEE Photon. Technol. Lett.*, vol. 22, no. 12, pp. 926–928, Jun. 15, 2010.
[2] Y. Ueda *et al.*, "4 x 4 InAlGaAs/InAlAs optical-switch fabric by cascading mach-zehnder interferometer-type optical switches with low-power and low-polarization-dependent operation," *IEEE Photon. Technol. Lett.*, vol. 24, pp. 757–759, May 1, 2012.
[3] G. Singh, A. Goyal, R. P. Yadav, and V. Janyani, "Modeling of a compact and completely non-blocking 4 × 4 multimode interference switch for optical communication applications," *Opt. Eng.*, vol. 51, May 2012.
[4] Z. Jin and G. D. Peng, "Optimal design of N × N silica multimode interference couplers—an improved approach," *Opt. Commun.*, vol. 241, pp. 299–308, Nov. 2004.
[5] W. Wang, H. Zhou, J. Yang, M. Wang, and X. Jiang, "Highly integrated 3 × 3 silicon thermo-optical switch using a single combined phase shifter for optical interconnects," *Opt. Lett.*, vol. 37, pp. 2307–2309, Jun. 15, 2012.
[6] M. Yang *et al.*, "Non-blocking 4 × 4 electro-optic silicon switch for on-chip photonic networks," *Opt. Exp.*, vol. 19, pp. 47–54, Jan. 3, 2011.
[7] J. Liu, J. Yu, S. Chen, and Z. Li, "Integrated folding 4 × 4 optical matrix switch with total internal reflection mirrors on SOI by anisotropic chemical etching," *IEEE Photon. Technol. Lett.*, vol. 17, no. 6, pp. 1187–1189, Jun. 2005.

[8] C.-T. Zheng, L. Liang, W.-L. Ye, D.-M. Zhang, and C.-S. Ma, "Silica/polymer TIR optical switches and a proposal for nonblocking four-port routers," *IEEE Photon. Technol. Lett.*, vol. 27, no. 6, pp. 581–584, Mar. 15 2015.
[9] L. Liang *et al.*, "Fabrication and characterization on an organic/inorganic 2 × 2 Mach-Zehnder interferometer thermo-optic switch," *Photon. Nanostruct.—Fundam. Appl.*, vol. 12, pp. 173–183, Apr. 2014.
[10] Q. Chen, F. Zhang, R. Ji, L. Zhang, and L. Yang, "Universal method for constructing N-port non-blocking optical router based on 2 × 2 optical switch for photonic networks-on-chip," *Opt. Exp.*, vol. 22, pp. 12614–12627, May 19, 2014.
[11] T. Goh *et al.*, "Low-loss and high-extinction-ratio silica-based strictly nonblocking 16 × 16 thermooptic matrix switch," *IEEE Photon. Technol. Lett.*, vol. 10, no. 6, pp. 810–812, Jun. 1998.
[12] T. Goh, A. Himeno, M. Okuno, H. Takahashi, and K. Hattori, "High-extinction ratio and low-loss silica-based 8 × 8 strictly nonblocking thermooptic matrix switch," *J. Lightw. Technol.*, vol. 17, no. 7, pp. 1192–1199, Jul. 1999.
[13] R. Kasahara *et al.*, "New structure of silica-based planar lightwave circuits for low-power thermooptic switch and its application to 8 × 8 optical matrix switch," *J. Lightw. Technol.*, vol. 20, no. 6, pp. 993–1000, Jun. 2002.
[14] Y. T. Han *et al.*, "N × N polymer matrix switches using thermo-optic total-internal-reflection switch," *Opt. Exp.*, vol. 20, pp. 13284–13295, Jun. 2012.
[15] H. Yu, X. Q. Jiang, J. Y. Yang, Y. Tang, and M. H. Wang, "2 × 3 Thermo-optical switch utilizing total internal reflection," *Appl. Phys. Lett.*, vol. 88, Jan. 2 2006.